Effective field theory for vector-like leptons and its collider signals

Mikael Chala [a], Paweł Kozów [a], Maria Ramos [a,b], Arsenii Titov [c,*]

[a] *CAFPE and Departamento de Física Teórica y del Cosmos, Universidad de Granada, E-18071 Granada, Spain*
[b] *Laboratório de Instrumentação e Física Experimental de Partículas, Departamento de Física da Universidade do Minho, Campus de Gualtar, 4710-057 Braga, Portugal*
[c] *Dipartimento di Fisica e Astronomia "G. Galilei", Università degli Studi di Padova and INFN, Sezione di Padova, Via Francesco Marzolo 8, I-35131 Padova, Italy*

A B S T R A C T

We argue that in models with several high scales; *e.g.* in composite Higgs models or in gauge extensions of the Standard Model (SM), vector-like leptons can be likely produced in a relatively large $\sqrt{s}$ region of the phase space. Likewise, they can easily decay into final states not containing SM gauge bosons. This contrasts with the topology in which these new particles are being searched for at the LHC. Adopting an effective field theory approach, we show that searches for excited leptons must be used instead to test this scenario. We derive bounds on all the relevant interactions of dimension six; the most constrained ones being of about 0.05 TeV^{-2}. We build new observables to improve current analyses and study the impact on all single-field UV completions of the SM extended with a vector-like lepton that can be captured by the effective field theory at tree level, in the current and in the high-luminosity phase of the LHC.

1. Introduction

Leptons beyond those of the Standard Model (SM), if they exist, have masses well above the electroweak (EW) scale, or else they would conflict with EW and Higgs precision data. Therefore, they can not get their masses from the Higgs mechanism. Instead, any such new lepton E must be vector-like with respect to the SM gauge symmetry $SU(3)_c \times SU(2)_L \times U(1)_Y$; namely the left-handed (LH) and right-handed (RH) components transform in the same representation, which allows an explicit mass term $M_E \overline{E} E$.

Direct searches for vector-like leptons (VLLs) are being performed at the LHC [1–7], with null results so far. This observation does not necessarily imply that there are no VLLs below the TeV scale. It can rather be that, contrary to what all the aforementioned experimental analyses presume, the actual VLLs *(i)* are mostly single produced, *(ii)* populate mainly the phase space of relatively large $\sqrt{s}$ and *(iii)* do not decay to SM gauge bosons.

This is indeed the case in several theoretical frameworks; for example in some composite Higgs models (CHMs). The latter involve a new strong sector that confines around the scale $f_* \sim$ TeV. While vector resonances are expected to have masses of order $\Lambda \sim g_* f_*$, with $g_* \gg 1$ being the coupling between composite res-

onances, fermionic resonances should rather lie at a scale closer to f_*, generating the hierarchy $m_E \ll \Lambda$. One reason is that EW precision data (EWPD) and flavour constraints are much stronger for vector than for fermionic resonances [8]. One additional reason is that the Higgs mass in CHMs is much more sensitive to m_E than to m_V, particularly in those in which the SM leptons interact sizeably with the strong sector. Such models, in turn, are motivated by the flavour anomalies [9–14].

It is therefore likely that the actual phenomenology of VLLs at the LHC must be described by an effective field theory (EFT),[1] including not only the dimension-four Yukawa interaction $\sim y \overline{l_L} H E$ (with l_L and H being the LH lepton doublet and the Higgs boson, respectively), but also dimension-six interactions suppressed by $1/\Lambda^2$. We note however that y modifies the Z coupling to the SM leptons and it is therefore very constrained by EWPD; $y \lesssim 0.1$ [18]. Moreover, in CHMs, $y \sim Y_* s_L s_R$ where Y_* is a proto-Yukawa coupling between the fully composite Higgs and the fermionic resonances and s_L and s_R are the degree of compositeness of LH and RH fermions. If Minimal Flavour Violation is at work, then s_L vanishes [19], and therefore $y \to 0$. Hence, the single production $pp \to E\ell$ mode populating the relatively large $\sqrt{s}$ phase space dominates, because the production cross section grows as $\sigma \sim s/\Lambda^4$.

---

* Corresponding author.
  E-mail address: arsenii.titov@pd.infn.it (A. Titov).

[1] For recent studies of the impact of higher-dimensional operators on the phenomenology of vector-like quarks, see Refs. [15–17].

Likewise, the non-resonant decay channel $E \to \ell q \overline{q}$ can dominate over $E \to Z/h\ell$ (or $W\nu$). Naive dimensional analysis tells us that this happens provided $y \lesssim 0.1 (m_E/\Lambda)^2$.[2]

Other scenarios that can be captured by the aforementioned EFT include $U(1)'$ extensions of the SM gauge group, in which a new vector boson Z' gets a mass from a hidden Higgs not charged under the SM. It is well known that new VLLs must be generally present to avoid gauge anomalies [22–24]. The mass of the latter is controlled by the Yukawas to the hidden Higgs and so it can be easily much smaller than the mass of the Z'.

In any case, in this paper we adopt an agnostic EFT approach to the physics of E. A thorough inspection of the experimental literature reveals that the search of Ref. [25], originally conceived for excited leptons, might be used to test this scenario. There are however severe limitations to translate the bounds obtained in that paper to our framework. To start with, only one dimension-six operator is considered in that experimental analysis. Second, it only considers the decay $E \to \ell q \overline{q}$, with q being a light quark, neither a b nor a top. And third, the bounds obtained in that search can not be translated to UV models with cut-off below 10 TeV. In order to overcome these weaknesses, we recast the experimental analysis in full detail and apply it to the entire EFT, for the different decay channels of E in a wide range of masses, while keeping strict control of the EFT validity.

The article is organised as follows. In section 2 we introduce the EFT for the SM extended with E (ESMEFT), and discuss its effects on single E production and the subsequent decay. In section 3 we recast the most up-to-date search for excited leptons and analyse the impact of the different effective operators involving E on its production and decay. We derive master formulae that can be used to automatically predict the number of events expected in any of the signal regions of the experimental search for *arbitrary* combinations of operators (all of which produce E at very different regions of the phase space). We discuss the validity of the EFT and derive global bounds on the Wilson coefficients of the EFT accordingly. In section 4 we discuss modifications of the current analysis that improve the sensitivity to the ESMEFT, at current and future luminosities. In section 5 we discuss different UV completions of the ESMEFT, particularly all those extending the SM+E renormalizable Lagrangian with just one single field, and apply our analyses to constrain their parameter spaces. We conclude in section 6. We dedicate appendix A to a discussion of the technical details on the perturbative unitarity limits that we use when studying the validity of the EFT.

2. Theoretical setup

We extend the SM with an $SU(2)_L$ singlet VLL $E = E_R + E_L$ with hypercharge $Y = -1$. The leading (renormalizable) Lagrangian reads

$$L = \overline{E} \left(i \slashed{D} - M_E \right) E - \left(y \overline{l_L} H E + \text{h.c.} \right) . \tag{1}$$

At dimension six, the following contact interactions contribute to $pp \to E\ell$:[3]

$$L = f_{ue} \left(\overline{u_R} \gamma^\mu u_R \right) \left(\overline{e_R} \gamma_\mu E \right) + f_{de} \left(\overline{d_R} \gamma^\mu d_R \right) \left(\overline{e_R} \gamma_\mu E \right)$$
$$+ f_{qe} \left(\overline{q_L} \gamma^\mu q_L \right) \left(\overline{e_R} \gamma_\mu E \right) + f_{qdl} \left(\overline{q_L} d_R \right) \left(\overline{E} l_L \right)$$
$$+ f_{qul} \left(\overline{q_L} u_R \right) \epsilon \left(\overline{l_L}^T E \right) + f_{luq} \left(\overline{l_L} u_R \right) \epsilon \left(\overline{q_L}^T E \right) + \text{h.c.} , \tag{2}$$

where $f_i \equiv c_i/\Lambda^2$. As usual, e_R denotes the SM lepton singlet; and u_R and d_R and q_L represent the SM singlet quarks and the LH doublet, respectively. We also define $\epsilon = i\sigma_2$, with σ_2 being the second Pauli matrix.

Remarkably, non four-fermion interactions lead to processes suppressed by loop or Yukawa factors or do not grow with energy; and they can therefore be neglected. (Evidently, although our research has been triggered by previous studies of CHMs, this EFT describes any new physics scenario involving such VLL, irrespectively of whether any other new physics is much heavier or not; it is hence more generic than the usual approach to the phenomenology of VLLs.)

The relations between interaction eigenstates e, E and the mass eigenstates e^-, E^- read

$$e_R = \cos\theta_R e_R^- + \sin\theta_R E_R^- ,$$
$$E_R = -\sin\theta_R e_R^- + \cos\theta_R E_R^- , \tag{3}$$

$$e_L = \cos\theta_L e_L^- + \sin\theta_L E_L^- ,$$
$$E_L = -\sin\theta_L e_L^- + \cos\theta_L E_L^- , \tag{4}$$

for the right and left chiral fields, respectively, where

$$\sin\theta_L \to \frac{yv}{\sqrt{2}m_E} , \qquad \sin\theta_R \to 0 , \tag{5}$$

for $y \ll 1$ and in the limit $m_e \to 0$. The relation between M_E and the physical mass m_E reads

$$M_E = \sqrt{m_E^2 - \frac{y^2 v^2}{2}} , \tag{6}$$

again, in the same limit. In what follows we shall denote $\cos\theta_L$ and $\sin\theta_L$ by c_L and s_L, respectively.

The mixing between the SM charged leptons and E modifies the coupling of the Z boson to the left current:

$$\frac{e}{s_W c_W} g_L \overline{e_L} \gamma^\mu e_L Z_\mu = \frac{e}{s_W c_W} \left(g_L^{SM} + \delta g_L \right) \overline{e_L} \gamma^\mu e_L Z_\mu , \tag{7}$$

where g_L^{SM} is the corresponding coupling in the SM, $\delta g_L = (yv/\sqrt{2}m_E)^2/2$, and s_W and c_W are the sine and cosine of the Weinberg angle, respectively. EWPD provide the following constraint on the mixing between the SM fermions and the new heavy VLL at the 95% CL [18]:

$$|s_L| = \left| \frac{yv}{\sqrt{2}m_E} \right| < 0.021 \, (0.030) , \tag{8}$$

for E mixing with electrons (muons). Taking for reference $m_E = 0.5$ TeV, the bound on y then reads

$$|y| < 0.06 \, (0.09) . \tag{9}$$

The regime $y \ll 1$ is therefore justified. The usual regime in which effective operators are ignored corresponds to $\Lambda \to \infty$. In both

---

[2] Note also that effective Higgs operators, *e.g.* $(H^\dagger i D_\mu H)(\overline{e}\gamma^\mu e)$ or $(H^\dagger i D_\mu H)(\overline{E}\gamma^\mu e)$, can be negligible. This happens for example when the lightest vector resonance at the scale Λ is the one associated to $U(1)_X$ in the minimal CHM [20] $SO(5) \times U(1)_X/SO(4) \times U(1)_X$, in which case it does not interact with the Higgs degrees of freedom before EW symmetry breaking [21]. For vector triplets of $SO(4)$, which do couple to the Goldstone bosons, the operator $(H^\dagger i D_\mu H)(\overline{E}\gamma^\mu e)$ arises with strength $\sim g_*^2 s_R/\Lambda^2$. We have checked that, in this case, the decay via effective operators still dominates provided 0.6 TeV $\lesssim m_E \lesssim 1$ TeV.

[3] Let us note that, within the context of CHMs, the Wilson coefficients f_{qdl}, f_{qul} and f_{luq} are expected to vanish for $y \to 0$, because either the LH or the RH

SM fermions should be fully elementary in this case. In general, SM four-fermion operators, $(qq)(\ell\ell)$ and $(qq)(qq)$ are also present. Bounds on these are comparable [26–28] or weaker [29] than those that we obtain below for the ESMEFT; but the corresponding operators are suppressed by one more power of the lepton degree of compositeness.
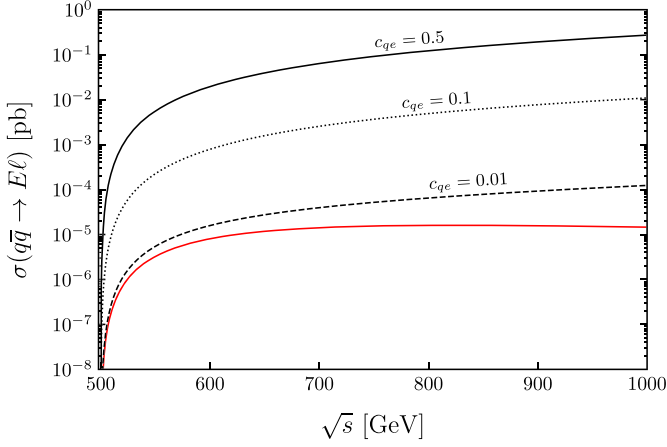
Fig. 1. Single production cross section as a function of $\sqrt{s}$, for $m_E = 500$ GeV and $y = 0.1$. The black lines correspond to different values of c_{qe}, with $\Lambda = 1$ TeV. All other Wilson coefficients are set to zero. The red line shows the cross section for the SM mediated process.

cases, the single production cross section triggered by $u\bar{u}$, to leading order in θ_W and having neglected $m_Z \ll \sqrt{s}$, reads

$$\frac{d\sigma}{d\theta} = \frac{\sin\theta}{32\pi s}\left(1 - \frac{m_E^2}{s}\right)\left\{-\frac{\pi^2\alpha^2}{3s_W^4 s^2}s_L^2(s+t)\left(m_E^2 - s - t\right)\right.$$
$$+ \frac{1}{3\Lambda^4}\left[s\left(s - m_E^2\right)\left(\frac{c_{qul}^2}{4} + c_{ue}^2\right)\right.$$
$$+ t\left(t - m_E^2\right)\left(\frac{c_{luq}^2}{4} + c_{ue}^2 + c_{qe}^2\right)$$
$$\left.\left.+ st\left(2c_{ue}^2 - \frac{1}{2}c_{qul}c_{luq}\right)\right]\right\}. \tag{10}$$

Likewise, for the counterpart driven by $d\bar{d}$ annihilation, we have the following result for the differential cross section:

$$\frac{d\sigma}{d\theta} = \frac{\sin\theta}{32\pi s}\left(1 - \frac{m_E^2}{s}\right)\left\{-\frac{\pi^2\alpha^2}{3s_W^4 s^2}s_L^2(s+t)\left(m_E^2 - s - t\right)\right.$$
$$+ \frac{1}{3\Lambda^4}\left[s\left(s - m_E^2\right)\left(\frac{c_{qdl}^2}{4} + c_{de}^2\right)\right.$$
$$\left.\left.+ t\left(t - m_E^2\right)\left(c_{qe}^2 + c_{de}^2\right) + 2stc_{de}^2\right]\right\}. \tag{11}$$

Integration over θ can be performed by noticing that $t = m_E^2 - 2p_i\left(\sqrt{m_E^2 + p_f^2} - p_f\cos\theta\right)$, with $p_i = \sqrt{s}/2$ and $p_f = (s - m_E^2)/(2\sqrt{s})$.

In Fig. 1 we present the total single production cross section for fixed values of the Wilson coefficient f_{qe} and assuming the maximum experimentally allowed value for y. For comparison, the red line shows the cross section for $\Lambda \to \infty$, in which the only contribution comes from the Z exchange. This s-channel contribution suppressed by the gauge boson propagator scales as $\sigma \sim 1/s$. On the contrary, in the EFT, $\sigma \sim s/\Lambda^4$ and therefore the cross section grows with the energy. Together with the y suppression, this effect makes the effective interactions dominate the cross section in the large $\sqrt{s}$ region, even for f_{qe} as small as ~ 0.01 TeV^{-2}.

The Yukawa coupling y in Eq. (1) triggers also the two-body decay of E into SM gauge bosons, $E \to Z/h\ell$ and $E \to W\nu$. For $y \ll 1$ and $m_Z \ll m_E$, the decay width reads

$$\Gamma = y^2\frac{\alpha}{16s_W^2 c_W^2}\left(\frac{v}{m_Z}\right)^2 m_E. \tag{12}$$

Concerning the three-body decay of E, let us first note that, if its interactions are flavour universal, then it couples equally to all quarks and leptons, and therefore E decays mostly into $\ell q\bar{q}$, with q being either a light, a bottom or a top quark; because there are three (colour) copies of each quark. Likewise, if similarly to the Higgs boson, E couples hierarchically to all fermions according to their masses, then its decays to three leptons is again subdominant. In light of this observation, we will neglect the mode $E \to \ell\ell\bar{\ell}$ hereafter. This implies that the operators relevant for analysing the decay of E are also precisely those in Eq. (2). The differential decay width for $E \to \ell u\bar{u}$ reads

$$\frac{d\Gamma'}{dE_1 dE_2} = \frac{3}{128\pi^3 m_E}\left[2E_1 m_E\left(m_E^2 - 2E_1 m_E\right)\left(f_{luq}^2 + 4f_{qe}^2\right)\right.$$
$$+ 2f_{luq}f_{qul}\left(m_E^2 - 2E_1 m_E\right)\left(m_E^2 - 2E_3 m_E\right)$$
$$+ 2E_3 f_{qul}^2 m_E\left(m_E^2 - 2E_3 m_E\right)$$
$$\left.+ 8E_2 f_{ue}^2 m_E\left(m_E^2 - 2E_2 m_E\right)\right]. \tag{13}$$

Analogously, for $E \to \ell d\bar{d}$ we have

$$\frac{d\Gamma'}{dE_1 dE_2} = \frac{3}{128\pi^3 m_E}\left[8E_1 f_{qe}^2 m_E\left(m_E^2 - 2E_1 m_E\right)\right.$$
$$+ 8E_2 f_{de}^2 m_E\left(m_E^2 - 2E_2 m_E\right)$$
$$\left.+ 2E_3 f_{qdl}^2 m_E\left(m_E^2 - 2E_3 m_E\right)\right], \tag{14}$$

where E_1, E_2 and E_3 are the energies of $u(d), \bar{u}(\bar{d})$ and ℓ, respectively. Upon integrating over the whole phase space, we arrive at

$$\Gamma' = \frac{m_E^5}{2048\pi^3}\left[f_{luq}^2 + f_{luq}f_{qul} + f_{qul}^2 + f_{qdl}^2\right.$$
$$\left.+ 4\left(2f_{qe}^2 + f_{ue}^2 + f_{de}^2\right)\right]. \tag{15}$$

Assuming $\mathcal{O}(1)$ couplings and all quarks, the comparison between Γ' and Γ reveals that the three-body decay dominates for $y \lesssim 0.2(m_E/\Lambda)^2$. Namely, $y \lesssim 0.008$ (0.02) for $\Lambda/m_E \sim 5$ (3). This value of y is very close to the EWPD bound, it is therefore very likely that E decays predominantly via EFT operators. Hereafter we study the regime $y \to 0$, and focus only on the case $\ell = \mu$. Departures from this assumption are discussed in section 6.

3. Collider signatures

In the regime $y \to 0$, the single production of E and its subsequent decays proceed as depicted in Fig. 2. The experimental analysis of Ref. [25] is optimised for the light quark channel, shown in the left panel (the one with $q\bar{q}$).

In general terms, it requires first two isolated leptons with $p_T > 35$ GeV (25 GeV) and $|\eta| < 1.44$ or $1.56 < |\eta| < 2.50$ ($|\eta| < 2.4$) for electrons (muons). (Isolation is defined by the requirement that the sum of the p_T of all tracks within $\Delta R = 0.3$ of a lepton is smaller than 5 GeV.) Likewise, it requires at least two anti-k_t ($R = 0.4$) jets with $p_T > 50$ GeV. The leading lepton is also required to have $p_T > 230$ GeV (53 GeV) for electrons (muons). Finally, the invariant mass of the two leptons must be above 500 GeV.
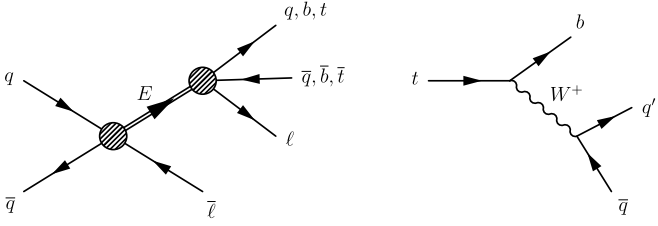
Fig. 2. Left: single production of E and its subsequent decay via four-fermion operators. Right: hadronic decay of the top in the SM.

The discriminating variable is the invariant mass of the two leptons and the two leading jets, $m_{\ell\ell jj}$. It is split into five energy bins: $[0.5 - 1.5]$ TeV, $[1.5 - 2.5]$ TeV, $[2.5 - 3.5]$ TeV, $[3.5 - 4.5]$ TeV, $[4.5 - 10]$ TeV.

In order to determine limits on f, we use the energy bin $[1.5 - 2.5]$ TeV, so that our EFT can be used to describe a wide range of UV models. (If we use all bins, models with $\Lambda < 10$ TeV can not be studied using the EFT approach.) Within this energy region, even f of order $\mathcal{O}(1)$ TeV^{-2} are allowed by perturbative unitarity constraints; see appendix A ($m_{\ell\ell jj}$ can be used as a proxy for the partonic centre-of-mass energy $\sqrt{\hat{s}}$).

Following Eqs. (10) and (11), the cross section, and therefore the number of events in each of these bins, can be written as

$$N = \frac{1}{\Lambda^4}\left[\mathcal{I}_1^u\left(\frac{c_{qul}^2}{4} + c_{ue}^2\right) + \mathcal{I}_2^u\left(\frac{c_{luq}^2}{4} + c_{ue}^2 + c_{qe}^2\right)\right.$$
$$+ \mathcal{I}_3^u\left(2c_{ue}^2 - \frac{1}{2}c_{qul}c_{luq}\right)$$
$$\left. + \mathcal{I}_1^d\left(\frac{c_{qdl}^2}{4} + c_{de}^2\right) + \mathcal{I}_2^d\left(c_{de}^2 + c_{qe}^2\right) + 2\mathcal{I}_3^d c_{de}^2\right], \quad (16)$$

where the coefficients $\mathcal{I}_i^q$, $q = u, d$, $i = 1, 2, 3$, are bin as well as mass dependent and must be obtained from simulation. To this aim we have generated signal events using MadGraph v5 [30] and Pythia v8 [31] for the three cases: $E \to \ell q\bar{q}$, $\ell b\bar{b}$, $\ell t\bar{t}$. To extract $\mathcal{I}_1^u$, $\mathcal{I}_2^u$ and $\mathcal{I}_3^u$, we turn on c_{qul}, c_{luq} and c_{ue}, respectively. Furthermore, we set $c_{de} \neq 0$ to realise the decay of E to the down-type quarks, whereas the semi-leptonic decay of E to a pair of tops is triggered by the operator responsible for the production of E. All other operator coefficients are set to zero. To obtain $\mathcal{I}_1^d$, $\mathcal{I}_2^d$ and $\mathcal{I}_3^d$, we turn on c_{qdl}, c_{qe} and c_{de}, respectively. The same operators trigger the decay of E to the down-type quarks. To allow for the decay of E to a pair of tops, we switch on c_{ue}, except for the second case, when $c_{qe} \neq 0$ already ensures such a decay.

The Monte Carlo events are subsequently passed through a recast version of the experimental analysis that we have implemented using dedicated routines based on Fastjet v3 [32] and ROOT v6 [33,34]. We do not include detector simulation. We have validated the analysis using the dominant background given by Drell-Yan production merged up to two extra matrix element partons, finding good agreement with the numbers provided in Ref. [25] (see Fig. 7 therein).

The coefficients $\mathcal{I}_i^q$ obtained in the way described above are shown in Tables 1, 2 and 3 for $m_E = 500$, 700 and 900 GeV, respectively. We focus on $\ell = \mu$; the (small) differences for electrons due to the different detector response are succinctly discussed in section 6.

Using these tables, we have compared the predicted number of signal events in each bin as derived from Eq. (16) to that obtained directly from simulation for $\mathcal{O}(100)$ different combinations of Wil-

son coefficients. The latter is always contained in a band of $\pm 15\%$ around the former.[4] We therefore take 15% as the systematic error in our prediction for the number of signal events.

We also report in Table 1 the number of observed events as well as the number of expected SM events as given in Ref. [25]. Using the CL$_s$ method [35], including the aforementioned 15% uncertainty on the signal as well as the uncertainties on the background, we derive the maximum number of allowed signal events in each bin. These numbers are also shown in the table.

We note that the coefficients $\mathcal{I}$ for light quarks and bottoms are roughly equivalent. (We will make use of this observation in what follows to derive bounds on the Wilson coefficients as a function of only $\mathcal{B}(E \to \ell j\bar{j}) \equiv \mathcal{B}(E \to \ell q\bar{q}) + \mathcal{B}(E \to \ell b\bar{b}) = 1 - \mathcal{B}(E \to \ell t\bar{t})$.) The main reason is that the final states in both cases are very similar and no b-tagging is at play.

The situation is very different for the top channel. The larger number of jets in the final state, together with the relatively small top quark leptonic branching ratio, makes the corresponding $\mathcal{I}$s even more than a factor of two smaller.

In Fig. 3 we show the limits on each of the operators of the EFT for $m_E = 500$ GeV and for $m_E = 900$ GeV. For setting bounds on f_{luq} we marginalise over f_{qul} (as they interfere among themselves); and *vice versa*. Note also that for these maximum values of f, the energy bin used in the analysis, $[1.5 - 2.5]$ TeV, is well within the energy regime of validity of the EFT in light of perturbative unitarity constraints; see appendix A.

4. Improvements and prospects

Extending the aforementioned experimental analysis with cuts on appropriate new observables can make it more sensitive to the ESMEFT. One such observable is the invariant mass of the reconstructed E. Note that, because E is heavy, it carries less momentum than the lepton in $pp \to E\ell$. Therefore, this lepton is typically the hardest one. This effect is strengthened by the fact that when E decays it releases energy to several particles.

Thus, one can reconstruct the four-momentum of E as the sum of the four-momenta of the softest lepton and the two hardest jets. The invariant mass of this object, m_E^{rec}, peaks well around the actual m_E when $\mathcal{B}(E \to \ell q\bar{q}) \sim 1$; see Fig. 4. (For this figure we assume $m_E = 700$ GeV. Given the low sensitivity of our previous results to m_E, and because it is in between the two extreme cases, $m_E = 500$ GeV and $m_E = 900$ GeV considered before, we restrict to this value hereafter.) The main background, ensuing from $Z + \text{jets}$ is also shown for comparison.

We extend the current analysis with the extra cut 650 GeV $< m_E^{\text{rec}} < 750$ GeV. In good approximation, the fraction of signal events that do not only pass all previous analysis cuts but also this extra one is bin and operator independent and of about 0.6. In the background, however, this number goes down to ~ 0.1.

The search has to be modified in a different way if one aims to be more sensitive to the case $\mathcal{B}(E \to \ell b\bar{b}) \sim 1$ or to $\mathcal{B}(E \to \ell t\bar{t}) \sim 1$. In the bottom channel, we require the presence of exactly two b-tagged jets. (In our simulation, b-jet candidates are selected among those jets with a B-meson within a cone of radius $\Delta R = 0.5$; the b-tagging efficiency is subsequently set to 0.7.) We then re-

---

[4] Note that in deriving Eq. (16), we have neglected the impact of the different effective operators triggering the decay of E on the efficiency of the analysis. The difference in the efficiencies for selecting single produced events in two samples that differ only by the operator driving the decay of E is small. Moreover, this difference tends to vanish if the two operators are linear combinations of $\{\mathcal{O}_{luq}, \mathcal{O}_{qe}, \mathcal{O}_{ue}\}$ or $\{\mathcal{O}_{de}, \mathcal{O}_{qe}\}$. The reason is that the differential E decay widths (see Eqs. (13) and (14)) driven by two operators within the same set differ only by $E_1 \leftrightarrow E_2$, while the cuts are the same for all jets. We have checked that this fact reflects well on the simulation.

Table 1
Coefficients $\mathcal{I}_i^q$, $q = u$ (d), in TeV^4 and rounded to two significant figures for $pp \to \mu^+\mu^- jj$ obtained upon recasting the experimental analysis of Ref. [25] for $\sqrt{s} = 13$ TeV and total integrated luminosity $\mathcal{L} = 77.4$ fb^{-1}. We have assumed $m_E = 500$ GeV and $\mathcal{B}(E \to \mu d\bar{d}) = 1$ (top), $\mathcal{B}(E \to \mu b\bar{b}) = 1$ (middle), and $\mathcal{B}(E \to \mu t\bar{t}) = 1$ (bottom). We also display the SM prediction, the data and the maximal allowed signal $s_{\max}$ in each bin (for muons in the final state). This latter number is computed using the CL$_s$ method, taking into account the uncertainty on the background displayed in the table as well as 15% uncertainty on the signal; see the text for details.

| | | Bins in $2\ell2j$ mass [TeV] | | | | |
		0.5 − 1.5	1.5 − 2.5	2.5 − 3.5	3.5 − 4.5	4.5 − 10
$E \to \mu d\bar{d}$	$\mathcal{I}_1^q/10^2$	390 (150)	530 (240)	220 (96)	62 (19)	22 (5.5)
	$\mathcal{I}_2^q/10^2$	140 (88)	180 (100)	74 (35)	19 (9.2)	8.4 (2.9)
	$\mathcal{I}_3^q/10^2$	−190 (−73)	−260 (−120)	−110 (−49)	−29 (−9.1)	−11 (−2.8)
$E \to \mu b\bar{b}$	$\mathcal{I}_1^q/10^2$	380 (150)	480 (210)	210 (88)	55 (22)	18 (3.5)
	$\mathcal{I}_2^q/10^2$	140 (85)	170 (97)	68 (33)	22 (7.4)	5.5 (2.1)
	$\mathcal{I}_3^q/10^2$	−190 (−79)	−240 (−110)	−100 (−44)	−29 (−11)	−9.2 (−1.7)
$E \to \mu t\bar{t}$	$\mathcal{I}_1^q/10^2$	170 (160)	200 (120)	73 (27)	20 (5.7)	4.3 (1.4)
	$\mathcal{I}_2^q/10^2$	93 (57)	85 (48)	24 (9.6)	5.3 (1.4)	1.0 (0.36)
	$\mathcal{I}_3^q/10^2$	−82 (−79)	−110 (−64)	−37 (−13)	−11 (−2.5)	−2.1 (−0.53)
SM		949 ± 115	161 ± 25	13.7 ± 3.7	1.2 ± 0.6	0.48 ± 0.32
Data		949	151	11	0	1
$s_{\max}$		291	60	14	4	5

Table 2
Coefficients $\mathcal{I}_i^q$, $q = u$ (d), in TeV^4 and rounded to two significant figures for $pp \to \mu^+\mu^- jj$ obtained upon recasting the experimental analysis of Ref. [25] for $\sqrt{s} = 13$ TeV and total integrated luminosity $\mathcal{L} = 77.4$ fb^{-1}. We have assumed $m_E = 700$ GeV and $\mathcal{B}(E \to \mu d\bar{d}) = 1$ (top), $\mathcal{B}(E \to \mu b\bar{b}) = 1$ (middle), and $\mathcal{B}(E \to \mu t\bar{t}) = 1$ (bottom).

| | | Bins in $2\ell2j$ mass [TeV] | | | | |
		0.5 − 1.5	1.5 − 2.5	2.5 − 3.5	3.5 − 4.5	4.5 − 10
$E \to \mu d\bar{d}$	$\mathcal{I}_1^q/10^2$	230 (79)	480 (210)	230 (100)	73 (30)	26 (7.5)
	$\mathcal{I}_2^q/10^2$	89 (57)	170 (96)	78 (39)	24 (10)	7.9 (2.0)
	$\mathcal{I}_3^q/10^2$	−110 (−40)	−240 (−110)	−110 (−51)	−35 (−15)	−12 (−3.4)
$E \to \mu b\bar{b}$	$\mathcal{I}_1^q/10^2$	260 (95)	460 (210)	200 (86)	74 (26)	21 (4.9)
	$\mathcal{I}_2^q/10^2$	94 (58)	160 (86)	68 (36)	20 (9.1)	6.5 (2.0)
	$\mathcal{I}_3^q/10^2$	−130 (−47)	−230 (−100)	−99 (−44)	−36 (−13)	−11 (−2.1)
$E \to \mu t\bar{t}$	$\mathcal{I}_1^q/10^2$	180 (150)	270 (160)	100 (50)	30 (11)	10 (2.6)
	$\mathcal{I}_2^q/10^2$	95 (60)	110 (57)	37 (17)	11 (4.2)	2.5 (0.53)
	$\mathcal{I}_3^q/10^2$	−85 (−74)	−140 (−82)	−52 (−25)	−16 (−5.6)	−5.2 (−1.2)

Table 3
Coefficients $\mathcal{I}_i^q$, $q = u$ (d), in TeV^4 and rounded to two significant figures for $pp \to \mu^+\mu^- jj$ obtained upon recasting the experimental analysis of Ref. [25] for $\sqrt{s} = 13$ TeV and total integrated luminosity $\mathcal{L} = 77.4$ fb^{-1}. We have assumed $m_E = 900$ GeV and $\mathcal{B}(E \to \mu d\bar{d}) = 1$ (top), $\mathcal{B}(E \to \mu b\bar{b}) = 1$ (middle), and $\mathcal{B}(E \to \mu t\bar{t}) = 1$ (bottom).

| | | Bins in $2\ell2j$ mass [TeV] | | | | |
		0.5 − 1.5	1.5 − 2.5	2.5 − 3.5	3.5 − 4.5	4.5 − 10
$E \to \mu d\bar{d}$	$\mathcal{I}_1^q/10^2$	120 (35)	400 (170)	210 (87)	72 (25)	29 (8.1)
	$\mathcal{I}_2^q/10^2$	43 (27)	150 (84)	68 (36)	25 (11)	9.7 (3.5)
	$\mathcal{I}_3^q/10^2$	−60 (−17)	−200 (−86)	−100 (−43)	−37 (−13)	−15 (−4.0)
$E \to \mu b\bar{b}$	$\mathcal{I}_1^q/10^2$	140 (51)	380 (170)	190 (81)	66 (23)	23 (5.7)
	$\mathcal{I}_2^q/10^2$	52 (33)	140 (78)	65 (33)	22 (8.7)	7.2 (2.3)
	$\mathcal{I}_3^q/10^2$	−68 (−25)	−190 (−86)	−94 (−41)	−33 (−11)	−11 (−2.6)
$E \to \mu t\bar{t}$	$\mathcal{I}_1^q/10^2$	110 (100)	230 (140)	100 (50)	34 (14)	12 (2.8)
	$\mathcal{I}_2^q/10^2$	64 (39)	100 (53)	38 (19)	12 (4.3)	2.7 (1.1)
	$\mathcal{I}_3^q/10^2$	−56 (−52)	−120 (−69)	−50 (−24)	−18 (−6.8)	−5.2 (−1.5)

construct E as the sum of the two leading b-jets and the softest lepton. The invariant mass of the reconstructed E is shown in Fig. 5 for both the signal and the main background, which in this case is $t\bar{t}$ (because the b-tagging requirement reduces Z + jets to negligible levels). In this case we require 550 GeV $< m_E^{\rm rec} <$ 700 GeV. The fraction of signal events surviving the new cuts is ~ 0.25, while for the background we get ~ 0.05.

Finally, in the top channel, in addition to requiring exactly two b-jets, we demand the presence of at least three light jets. We subsequently reconstruct E as the sum of the softest lepton, the two b-jets and the main three light jets. The corresponding $m_E^{\rm rec}$ is depicted in Fig. 6 in the signal and in $t\bar{t}$. We require in this case

500 GeV $< m_E^{\rm rec} <$ 800 GeV. The fraction of signal (background) events surviving the new extra cuts is ~ 0.2 (0.05). These numbers reflect the smaller difference between signal and background in this case.

Using the CL$_s$ method, assuming again a 15% uncertainty on the signal and the same uncertainties as before for the background, and assuming the data to be well described by the SM, we obtain the values of $s_{\max}$ shown in Table 4. They also include the numbers for the high-luminosity phase of the LHC (HL-LHC), in which the collected luminosity will reach $\mathcal{L} = 3$ ab^{-1}. Using these numbers, we demonstrate that the improved analyses can strengthen the sensitivity on f by more than 50%; see Table 5.
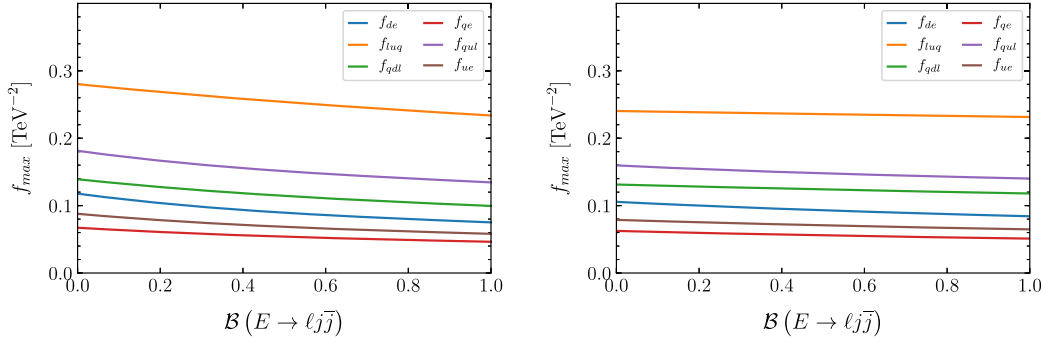
Fig. 3. The global limits on the EFT coefficients f for $m_E = 0.5$ TeV (left) and $m_E = 0.9$ TeV (right), using the second bin defined in Tables 1 and 3.
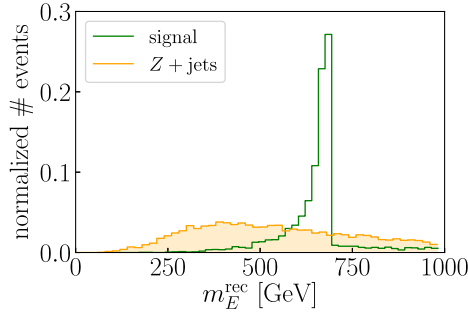

Fig. 4. Normalized distribution of $m_E^{\rm rec}$ right after the cut on $m_{\ell^+\ell^-} > 500$ GeV, in the signal for $\mathcal{B}(E \to \mu q \bar{q}) = 1$ and in the main background.
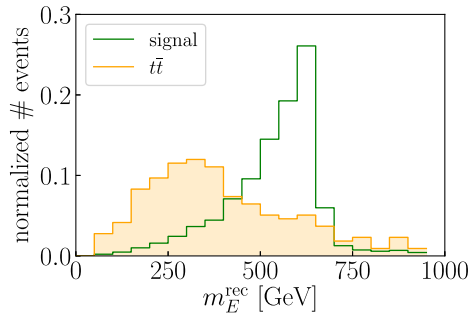

Fig. 5. Normalized distribution of $m_E^{\rm rec}$ right after the cut on $m_{\ell^+\ell^-} > 500$ GeV and after requiring exactly two b-jets, in the signal for $\mathcal{B}(E \to \mu b \bar{b}) = 1$ and in the main background.
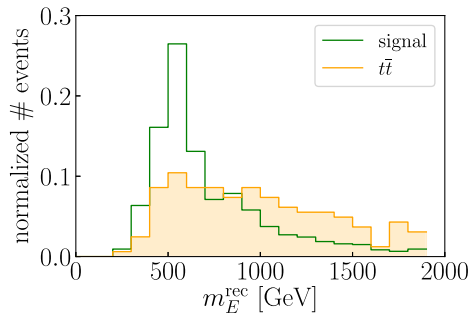

Fig. 6. Normalized distribution of $m_E^{\rm rec}$ right after the cut on $m_{\ell^+\ell^-} > 500$ GeV and after requiring exactly two b-jets and at least three light jets, in the signal for $\mathcal{B}(E \to \mu t \bar{t}) = 1$ and in the main background.

5. Applications

The single-field extensions of the SM+E that contribute to the EFT at tree level are summarised in Table 6. The names of the new

Table 4
Values of $s_{\rm max}$ in four signal regions of the improved analyses with collected luminosity of $\mathcal{L} = 77.4$ fb^{-1} (HL-LHC with $\mathcal{L} = 3$ ab^{-1}).

	Bins in $2\ell 2j$ mass [TeV]			
	$0.5 - 1.5$	$1.5 - 2.5$	$2.5 - 3.5$	$3.5 - 4.5$
$E \to \ell q \bar{q}$	46 (549)	14 (210)	5 (84)	4 (68)
$E \to \ell b \bar{b}$	14 (210)	6 (101)	4 (68)	4 (68)
$E \to \ell t \bar{t}$	14 (210)	6 (101)	4 (68)	4 (68)

Table 5
Bounds on the Wilson coefficients rounded to two significant figures, in TeV^{-2}, in the current and improved (future) analyses. We have assumed $m_E = 700$ GeV and used the energy bin $[1.5 - 2.5]$ TeV.

	$\mathcal{B}(E \to \mu q \bar{q}) = 1$	$\mathcal{B}(E \to \mu b \bar{b}) = 1$	$\mathcal{B}(E \to \mu t \bar{t}) = 1$
f_{ue}	0.060, 0.037 (0.023)	0.060, 0.038 (0.025)	0.076, 0.050 (0.035)
f_{de}	0.079, 0.049 (0.031)	0.081, 0.051 (0.034)	0.100, 0.072 (0.047)
f_{qe}	0.048, 0.030 (0.019)	0.049, 0.031 (0.021)	0.060, 0.042 (0.028)
f_{qdl}	0.110, 0.066 (0.041)	0.110, 0.067 (0.044)	0.120, 0.085 (0.056)
f_{qul}	0.130, 0.082 (0.051)	0.130, 0.083 (0.055)	0.160, 0.110 (0.072)
f_{luq}	0.220, 0.140 (0.086)	0.220, 0.140 (0.093)	0.240, 0.170 (0.110)

scalars follow Ref. [36], and those of the new vectors Ref. [37]. In general, more than one EFT operator is generated. Assuming $m_E = 700$ GeV, we can use Eq. (16) together with Table 2 and the values of $s_{\rm max}$ reported in Tables 1 and 4 to derive bounds on the space of couplings for a fixed mass of the heavy mediator (set to 5 TeV), taking *all* operators into account.

Assuming for simplicity that all couplings not involving E are equal, we show these results for the scalar mediators in Fig. 7. We also show for comparison the bounds from low-energy data and dijet searches [36]. Interestingly, *e.g.* in the case of ω_1, we see that for sufficiently large values of y^{Eu}, the bound on $y^{ql} = y^{eu}$ from our study is about 6 times more stringent than that from other data, and it can be improved by a factor of two at the HL-LHC. Despite not being explicitly shown, results for vector boson extensions of the SM+E are similar. Let us also note that, even for these masses, resonant searches are not necessarily more constraining. The reasons are: *(i)* Several of the mediators above proceed in t-channel, therefore not manifesting as peaks in the distribution of the total invariant mass. *(ii)* Even s-channel mediators can in general decay into other final states, probably harder to detect (*e.g.* invisible), which can even dominate the decay width; the EFT approach is insensitive to these effects. Evidently, for mediator masses above 10 TeV, the EFT approach is indisputable.

In good approximation, our results can also be easily extended to four-fermion operators involving only second and third generation quarks. For example, due to the PDF suppression, the cross section for single E production initiated by bottom quarks is about two orders of magnitude smaller than that initiated by down quarks. Therefore, it is expected that values of the Wilson coefficients f ten times larger can be probed at the LHC. Note that the

Table 6

The relevant Lagrangian for a scalar σ is $L = \partial_\mu \sigma^\dagger \partial^\mu \sigma - m_\sigma^2 \sigma^\dagger \sigma - (\sigma^\dagger J_\sigma + \text{h.c.})$. For a vector V we have instead $L = -\partial_\mu V_\nu^\dagger \partial^{[\mu} V^{\nu]} + m_V^2 V_\mu^\dagger V^\mu - (V^{\mu\dagger} J_\mu^V + \text{h.c.})$. For each row in the top (bottom) part of the table, $m = m_\sigma$ (m_V).

| Field	Relevant fermionic current	Wilson coefficients		
$\varphi \sim (1,2)_{\frac{1}{2}}$	$J = y^E \overline{E} l_L + y^d \overline{d_R} q_L + y^u i\sigma_2 \overline{q_L}^T u_R$	$f_{qdl} = \dfrac{y^d y^E}{m^2}$,	$f_{qul} = -\dfrac{y^u y^E}{m^2}$	
$\omega_1 \sim (3,1)_{-\frac{1}{3}}$	$J = y^{Eu} \overline{E^c} u_R + y^{ql} \overline{q_L^c} i\sigma_2 l_L + y^{eu} \overline{e_R^c} u_R$	$f_{ue} = \dfrac{y^{Eu} y^{eu}}{2m^2}$,	$f_{qul} = -\dfrac{y^{Eu} y^{ql}}{m^2}$,	$f_{luq} = \dfrac{y^{Eu} y^{ql}}{m^2}$
$\omega_4 \sim (3,1)_{-\frac{4}{3}}$	$J = y^{Ed} \overline{E^c} d_R + y^{ed} \overline{e_R^c} d_R$	$f_{de} = \dfrac{y^{Ed} y^{ed}}{2m^2}$		
$\Pi_7 \sim (3,2)_{\frac{7}{6}}$	$J = y^{Eq} \overline{E} q_L + y^{lu} i\sigma_2 \overline{l_L}^T u_R + y^{eq} \overline{e_R} q_L$	$f_{qe} = -\dfrac{y^{Eq} y^{eq}}{2m^2}$,	$f_{luq} = -\dfrac{y^{Eq} y^{lu}}{m^2}$	
$\mathcal{B}_\mu \sim (1,1)_0$	$J_\mu = g^E \overline{e_R} \gamma_\mu E + g^u \overline{u_R} \gamma^\mu u_R + g^d \overline{d_R} \gamma^\mu d_R$	$f_{de} = -\dfrac{g^E g^d}{m^2}$,	$f_{ue} = -\dfrac{g^E g^u}{m^2}$,	
	$+ g^q \overline{q_L} \gamma^\mu q_L$	$f_{qe} = -\dfrac{g^E g^q}{m^2}$		
$\mathcal{U}_\mu^2 \sim (3,1)_{\frac{2}{3}}$	$J_\mu = g^{Ed} \overline{E} \gamma_\mu d_R + g^{lq} \overline{l_L} \gamma_\mu q_L + g^{ed} \overline{e_R} \gamma_\mu d_R$	$f_{de} = -\dfrac{g^{Ed} g^{ed}}{m^2}$,	$f_{qdl} = \dfrac{2g^{lq} g^{Ed}}{m^2}$	
$\mathcal{U}_\mu^5 \sim (3,1)_{\frac{5}{3}}$	$J_\mu = g^{Eu} \overline{E} \gamma_\mu u_R + g^{eu} \overline{e_R} \gamma_\mu u_R$	$f_{ue} = -\dfrac{g^{Eu} g^{eu}}{m^2}$		
$\mathcal{Q}_\mu^5 \sim (3,2)_{-\frac{5}{6}}$	$J_\mu = g^{Eq} \overline{E^c} \gamma_\mu q_L + g^{dl} \overline{d_R^c} \gamma_\mu l_L + g^{eq} \overline{e_R^c} \gamma_\mu q_L$	$f_{qe} = \dfrac{g^{Eq} g^{eq}}{m^2}$,	$f_{qdl} = -\dfrac{2g^{Eq} g^{dl}}{m^2}$	
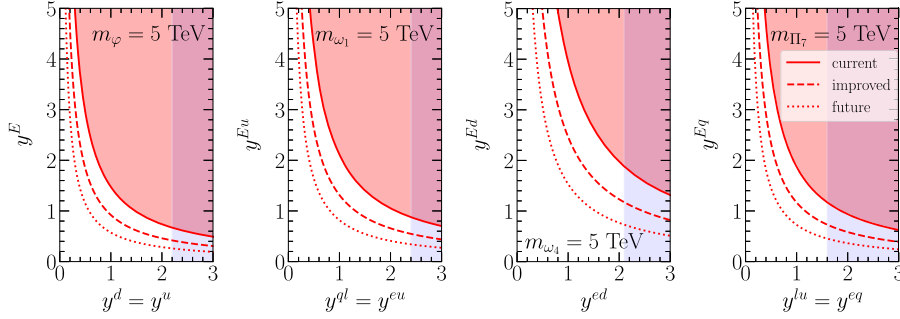
Fig. 7. Constraints on the couplings of the scalar UV completions of the ESMEFT derived under the assumption that all couplings to the SM fields in a given model are equal. We have used Eq. (16) along with the values of $\mathcal{I}$s from Table 2 and those of s_{max} from Tables 1 and 4, assuming the light quark decay channel of E and the second bin. "Current", "improved" ("future") refer to the developed LHC (HL-LHC) analyses described in the text. The light blue regions are excluded from EWPD or dijet searches at the LHC [36].

EFT is still valid in this case if we still restrict to $m_{\ell\ell jj} < 2.5$ TeV; see appendix A.

This observation can be used to explore the sensitivity to other models. For concreteness, following Ref. [14], let us consider the SM+E extension with a full singlet vector boson V with mass m_V and couplings

$$L = V^\mu \Big[g_{Vqq} \overline{q_L^3} \gamma_\mu q_L^3 + g_{VE\ell} \big(\overline{E} \gamma_\mu \mu_R + \text{h.c.} \big) \Big] + \dots . \quad (17)$$

The ellipsis encode terms not relevant for us, such as light lepton couplings to V, etc.

We fix $g_{Vqq} \sim 0.05 m_V^2 / \text{TeV}^2$. In the original reference this value is motivated by the flavour anomalies [38–44]. We keep the strong coupling $g_{VE\ell}$ free; while in the original reference it is fixed to 2.5. (The phenomenology studied there is not very sensitive to the value of this coupling.)

Upon integrating V out, the only ESMEFT operator (relevant for single production) generated is $\mathcal{O}_{qe}$, with

$$f_{qe} = -\frac{g_{Vqq} g_{VE\ell}}{m_V^2} \sim -0.05 g_{VE\ell} \, \text{TeV}^{-2}. \quad (18)$$

To compare the complementarity between our current analysis and that of Ref. [14], let us assume that E decays equally into SM gauge bosons and via the four-fermion operators. Thus, the region that can be probed at the HL-LHC following Ref. [14] (see right panel

of Fig. 5 therein) is depicted in blue in Fig. 8. The area below the line $m_V = 2m_E$, in which an on-shell produced V decays into $\overline{E}E$, is not accessible within that analysis. Due to the resonant nature of that search, the region above $m_V = 2.5$ TeV remains open.

On the other hand, within our current analysis in the bin $[1.5 - 2.5]$ TeV, we can probe values of f_{qe} of order 0.3 TeV^{-2} at the HL-LHC, which corresponds to $g_{VE\ell} \sim 6$. (This value is significantly smaller if E decays only via four-fermions; in which case the analysis of Ref. [14] is not sensitive to the model.) Notably, this constraint is m_V-independent, provided $m_V > 2.5$ TeV so that the EFT approach is valid. The corresponding bound is shown in red in Fig. 8.[5]

Thus, we can conclude that for sufficiently large $g_{VE\ell}$, our analysis together with that in Ref. [14] can completely probe the corresponding explanation of the flavour anomalies.

6. Conclusions

Using an effective field theory (EFT) approach, we have argued that, differently to what current searches for vector-like leptons

---

[5] We are making the conservative assumption that within our current analysis we are equally sensitive to values of m_E above our higher benchmark of $m_E = 900$ GeV. In light of the experimental results in Ref. [25], it is expected that the sensitivity to heavier E could be even better.
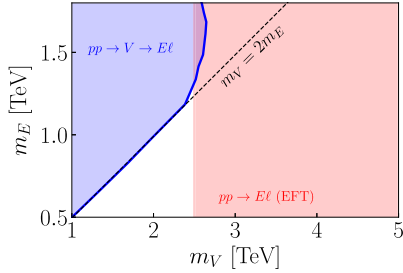
Fig. 8. Reach of the LHC to the model described in Eq. (17) using the resonant analysis of Ref. [14] (blue) versus the reach using the EFT analysis described in this article (red); see text for details.

(VLLs) E assume, E can be produced at high values of $\sqrt{s}$ via four-fermion interactions at the LHC. They can also decay as $E \to \ell q \bar{q}$ with *no* intermediate Standard Model (SM) gauge bosons.

We have shown that there are other (few) experimental analyses, most importantly searches for excited leptons [25], that are very sensitive to our hypothesis. They are however limited in scope, because they focus only on the case $q = u, d, c, s$ leaving bottom and top quarks aside, as well as a single four-fermion operator. Moreover, the statistical analysis in Ref. [25] does not apply to models with further particles below 10 TeV. Likewise, interpreting their bounds on ESMEFT operators involving only sea quarks breaks the EFT validity. (These objections apply also to other previous similar analyses [2,45].)

Thus, we have worked out the most generic base of EFT contact interactions involving E to dimension six. Upon recasting the experimental analysis of Ref. [25], we have obtained global bounds on all the EFT directions, for light, bottom and top quarks separately. To this aim, we have restricted to events with $\sqrt{s}$ below the threshold determined by perturbative unitarity, that we have also derived. Our findings show that Wilson coefficients as small as 0.05 TeV^{-2} are already ruled out in the muon channel.

For comparison, Ref. [25], which uses all energy bins to 10 TeV, reports $\Lambda \sim 20$ TeV for couplings of order 2π (and $m_E \sim$ TeV). This translates to $f \sim 0.015$ TeV^{-2}.

In the electron channel, our bounds on the Wilson coefficients are only slightly altered. Taking, for example, $m_E = 500$ GeV and using the energy bin $[1.5 - 2.5]$ TeV, the bounds on f_{qe} for muons and for electrons read, respectively, 0.046 (0.067) TeV^{-2} and 0.048 (0.070) TeV^{-2}, for E decaying into light and bottom jets (tops).

We have also modified the current analysis with cuts on new observables (most importantly the number of b-tagged jets and the reconstructed mass of E); improving the aforementioned bounds by a factor of ~ 1.6 (~ 1.4) for light and bottom quarks (tops).

Finally, we have applied our findings to concrete UV completions of the SMEFT extended with E. In particular, we have classified all possible single field extensions of the SM+E that induce the four-fermion interactions of interest at tree level. The limits on the couplings of these fields to purely SM currents can overcome those from low-energy data and dijet searches at the LHC by almost an order of magnitude with the improved analysis.

Altogether, our work motivates different searches for VLLs, that might be implemented by small modifications of current searches for excited leptons.

Declaration of competing interest

The authors declare that they have no known competing financial interests or personal relationships that could have appeared to influence the work reported in this paper.

Appendix A. Perturbative unitarity bounds

The aim of this appendix is to discuss the validity of the EFT approach. To this end, we first sum up the perturbative unitarity condition and apply it to the tree-level EFT amplitudes $q\bar{q} \to E\bar{\ell}$. More specifically, we derive constraints on the maximum partonic centre-of-mass energy $\hat{s}$ at which the EFT is applicable as a function of the Wilson coefficient f of each operator.

The unitarity of the S matrix, $SS^\dagger = 1$, together with the requirement of perturbativity imply that the partial waves $\mathcal{T}_j$ in the following partial wave decomposition of inelastic scattering amplitudes

$$\mathcal{M} = 16\pi \sum_J^\infty (2J+1) \mathcal{T}_{\lambda_1',\lambda_2';\lambda_1,\lambda_2}^{(J)}(\hat{s}) \, d_{\mu,\nu}^{(J)*}(\theta),\tag{19}$$

should fulfil the condition

$$\left| \mathcal{T}_{\lambda_1'\lambda_2';\lambda_1\lambda_2}^{(J)}(\hat{s}) \right| \le \frac{1}{2}\tag{20}$$

for each $J \in \{J_{\min}, J_{\min} + 1, \ldots\}$. In this expression, $\lambda_{1,2}$ and $\lambda_{1,2}'$ are the helicities of the initial and final particles, respectively; $\mu = \lambda_1 - \lambda_2$, $\nu = \lambda_1' - \lambda_2'$; $d^{(J)}$ are the Wigner matrices in the limit of azimuthal scattering angle $\phi \to 0$, and $J_{\min} = \max\{|\lambda_1 - \lambda_2|, |\lambda_1' - \lambda_2'|\}$. For more details on the partial wave unitarity condition, see *e.g.* Ref. [46].

Since the EFT amplitudes grow with the energy $\hat{s}$, so do the partial waves. We define the distinguished energy scale $\sqrt{\hat{s}^U}$ as the one that saturates the condition in Eq. (20):

$$\left| \mathcal{T}_{\lambda_1'\lambda_2';\lambda_1\lambda_2}^{(J)}(\hat{s}^U) \right| = \frac{1}{2}.\tag{21}$$

Importantly, $\hat{s}^U$ is a function of f. Given that for energies above $\hat{s}^U$ the EFT amplitudes are ill-defined, $\hat{s}^U$ defines the upper bound on $\hat{s}$ for which the EFT approach is valid.

Typically, the first partial wave yields the strongest unitarity bounds on $\hat{s}$. Correspondingly, we derive the bounds using $\mathcal{T}^{(J_{\min})}$. Since in our study the global bounds on f are expressed in terms of each Wilson coefficient f separately, we compute the unitarity bounds using one operator at a time. The J-th partial wave projections are computed using the orthogonality of the Wigner functions:

$$\mathcal{T}_{\mu,\nu}^{(J)} = \frac{1}{32\pi} \int_{-1}^1 d\cos\theta \, d_{\mu,\nu}^{(J)}(\theta) \, \mathcal{M}.\tag{22}$$

More specifically, for each operator we consider all helicity $q\bar{q} \to E\bar{\ell}$ amplitudes, where $q = u, d$, that are non-vanishing in the relativistic limit. For each such helicity combination we project the

Table 7

Solutions for $\sqrt{\hat{s}^U}$ (in TeV) from tree-level partial wave unitarity in the presence of a single operator at a time, for different values of the Wilson coefficients f. The examined processes are $u\bar{u} \to E\bar{\ell}$, $d\bar{d} \to E\bar{\ell}$.

f [TeV^{-2}]	f_{ue}	f_{de}	f_{qe}	f_{qdl}	f_{qul}	f_{luq}
10	1.9	1.9	1.9	1.6	1.6	2.2
1	6.1	6.1	6.1	5.0	5.0	7.1
0.1	19	19	19	16	16	22
0.01	61	61	61	50	50	71

Table 8

Same as Table 7 but for different values of the Wilson coefficients f.

f [TeV^{-2}]	f_{ue}	f_{de}	f_{qe}	f_{qdl}	f_{qul}	f_{luq}
0.3	11	11	11	9.2	9.2	13
0.25	12	12	12	10	10	14
0.2	14	14	14	11	11	16
0.15	16	16	16	13	13	18
0.1	19	19	19	16	16	22
0.075	22	22	22	18	18	26
0.06	25	25	25	20	20	29
0.05	27	27	27	22	22	32

amplitude $\mathcal{M}$ onto the $J_{\min}$ partial wave and derive the corresponding bound on $\hat{s}$. Finally, we identify $\hat{s}^U$ as the lowest among all such bounds.

Unitarity bounds for different values of f are presented in Table 7. For example, for $f = 1$ TeV^{-2} the bounds are in the range $\sqrt{\hat{s}^U} \in [5 - 7]$ TeV, depending on the operator involved.

For completeness, let us comment on the values of c in $f = c/\Lambda^2$ setting $\Lambda = \sqrt{\hat{s}^U}$, for different values of f and for each effective operator. Independently of the value of f, we obtain that $\sqrt{c} = 6.1$ for $f = f_{ue}, f_{de}, f_{qe}$; $\sqrt{c} = 5$ for $f = f_{qdl}, f_{qul}$; and $\sqrt{c} = 7.1$ for $f = f_{luq}$.

Note that, for a fixed f, $\Lambda = \sqrt{\hat{s}^U}$ can be (roughly) identified with the upper bound on the scale Λ. (The new physics scale in a UV completion should not be significantly separated from $\sqrt{\hat{s}^U}$ because it is responsible for unitarization of the complete amplitudes.) Therefore for a given f, the value of c, assuming $\Lambda = \sqrt{\hat{s}^U}$, is an approximate upper bound on the corresponding UV coupling.

Interestingly, the aforementioned values of c are *(i)* independent of the value of f and *(ii)* in the range between 1 and 4π, hence indeed close to the perturbative regime (as required by the perturbative unitarity condition).

Given this, a discussion on the EFT consistency of the analyses in sections 3 and 4 is in order. We note that the larger the value of f, the stronger the unitarity bounds. Thus, in particular, for the largest f within the limits, the $\sqrt{\hat{s}^U}$ should not be lower than the chosen cut-off on the (proxy) variable $m_{\ell\ell jj}$. Otherwise one uses events outside the validity of the EFT amplitudes while setting limits on the effective coefficients f; turning them to be not suitable for EFT interpretation.

In Table 8 we present the unitarity bounds as function of f for the values relevant for the 2.5 TeV cut-off case. Comparing the table with Fig. 3 one can see that all limits on f correspond to unitarity bounds that are not lower than the 2.5 TeV cut-off. Hence the limits are EFT interpretable. More explicitly, unitarity bounds $\sqrt{\hat{s}^U}$ that *e.g.* correspond to f from the first column in Table 5 read 25, 22, 27, 16, 13 and 16 TeV for $f_{ue}, f_{de}, f_{qe}, f_{qdl}, f_{qul}$ and f_{luq}, respectively.

References

[1] ATLAS collaboration, Search for type-III Seesaw heavy leptons in pp collisions at $\sqrt{s} = 8$ TeV with the ATLAS detector, Phys. Rev. D 92 (2015) 032001, arXiv:1506.01839.

[2] CMS collaboration, Search for excited leptons in proton-proton collisions at $\sqrt{s} = 8$ TeV, J. High Energy Phys. 03 (2016) 125, arXiv:1511.01407.

[3] ATLAS collaboration, Search for heavy lepton resonances decaying to a Z boson and a lepton in pp collisions at $\sqrt{s} = 8$ TeV with the ATLAS detector, J. High Energy Phys. 09 (2015) 108, arXiv:1506.01291.

[4] ATLAS collaboration, Searches for leptoquarks and heavy leptons with the ATLAS detector at the LHC, PoS EPS-HEP2015 (2015) 096.

[5] CMS collaboration, Search for vector-like leptons in multilepton final states in proton-proton collisions at $\sqrt{s} = 13$ TeV, Phys. Rev. D 100 (2019) 052003, arXiv:1905.10853.

[6] G. Aad, et al., ATLAS, arXiv:2008.07949 [hep-ex].

[7] CMS collaboration, Search for physics beyond the standard model in multilepton final states in proton-proton collisions at $\sqrt{s} = 13$ TeV, J. High Energy Phys. 03 (2020) 051, arXiv:1911.04968.

[8] M. Chala, J. Juknevich, G. Perez, J. Santiago, The elusive gluon, J. High Energy Phys. 01 (2015) 092, arXiv:1411.1771.

[9] C. Niehoff, P. Stangl, D.M. Straub, Violation of lepton flavour universality in composite Higgs models, Phys. Lett. B 747 (2015) 182, arXiv:1503.03865.

[10] C. Niehoff, P. Stangl, D.M. Straub, Direct and indirect signals of natural composite Higgs models, J. High Energy Phys. 01 (2016) 119, arXiv:1508.00569.

[11] A. Carmona, F. Goertz, Lepton flavor and nonuniversality from minimal composite Higgs setups, Phys. Rev. Lett. 116 (2016) 251801, arXiv:1510.07658.

[12] A. Carmona, F. Goertz, Eur. Phys. J. C 78 (11) (2018) 979, https://doi.org/10.1140/epjc/s10052-018-6437-1, arXiv:1712.02536 [hep-ph].

[13] F. Sannino, P. Stangl, D.M. Straub, A.E. Thomsen, Flavor physics and flavor anomalies in minimal fundamental partial compositeness, Phys. Rev. D 97 (2018) 115046, arXiv:1712.07646.

[14] M. Chala, M. Spannowsky, Behavior of composite resonances breaking lepton flavor universality, Phys. Rev. D 98 (2018) 035010, arXiv:1803.02364.

[15] J.C. Criado, M. Perez-Victoria, Vector-like quarks with non-renormalizable interactions, J. High Energy Phys. 01 (2020) 057, arXiv:1908.08964.

[16] J.H. Kim, I.M. Lewis, Loop induced single top partner production and decay at the LHC, J. High Energy Phys. 05 (2018) 095, arXiv:1803.06351.

[17] H. Alhazmi, J.H. Kim, K. Kong, I.M. Lewis, Shedding light on top partner at the LHC, J. High Energy Phys. 01 (2019) 139, arXiv:1808.03649.

[18] J. de Blas, Electroweak limits on physics beyond the standard model, EPJ Web Conf. 60 (2013) 19008, arXiv:1307.6173.

[19] M. Redi, Leptons in composite MFV, J. High Energy Phys. 09 (2013) 060, arXiv:1306.1525.

[20] K. Agashe, R. Contino, A. Pomarol, The minimal composite Higgs model, Nucl. Phys. B 719 (2005) 165, arXiv:hep-ph/0412089.

[21] G. Panico, A. Wulzer, The Composite Nambu-Goldstone Higgs, vol. 913, Springer, 2016, arXiv:1506.01961.

[22] M. Duerr, P. Fileviez Perez, M.B. Wise, Gauge theory for baryon and lepton numbers with leptoquarks, Phys. Rev. Lett. 110 (2013) 231801, arXiv:1304.0576.

[23] W. Chao, Symmetries behind the 750 GeV diphoton excess, Phys. Rev. D 93 (2016) 115013, arXiv:1512.06297.

[24] M. Chala, M. Duerr, F. Kahlhoefer, K. Schmidt-Hoberg, Tricking Landau–Yang: how to obtain the diphoton excess from a vector resonance, Phys. Lett. B 755 (2016) 145, arXiv:1512.06833.

[25] CMS collaboration, Search for an excited lepton that decays via a contact interaction to a lepton and two jets in proton-proton collisions at $\sqrt{s} = 13$ TeV, J. High Energy Phys. 05 (2020) 052, https://doi.org/10.1007/JHEP05(2020)052, arXiv:2001.04521.

[26] J. de Blas, M. Chala, J. Santiago, Global constraints on lepton-quark contact interactions, Phys. Rev. D 88 (2013) 095011, arXiv:1307.5068.

[27] A. Falkowski, M. González-Alonso, K. Mimouni, Compilation of low-energy constraints on 4-fermion operators in the SMEFT, J. High Energy Phys. 08 (2017) 123, arXiv:1706.03783.

[28] A. Greljo, D. Marzocca, High-p_T dilepton tails and flavor physics, Eur. Phys. J. C 77 (2017) 548, arXiv:1704.09015.

[29] O. Domenech, A. Pomarol, J. Serra, Probing the SM with dijets at the LHC, Phys. Rev. D 85 (2012) 074030, arXiv:1201.6510.

[30] J. Alwall, R. Frederix, S. Frixione, V. Hirschi, F. Maltoni, O. Mattelaer, et al., The automated computation of tree-level and next-to-leading order differential cross sections, and their matching to parton shower simulations, J. High Energy Phys. 07 (2014) 079, arXiv:1405.0301.

[31] T. Sjöstrand, S. Ask, J.R. Christiansen, R. Corke, N. Desai, P. Ilten, et al., An introduction to PYTHIA 8.2, Comput. Phys. Commun. 191 (2015) 159, arXiv:1410.3012.

[32] M. Cacciari, G.P. Salam, G. Soyez, FastJet user manual, Eur. Phys. J. C 72 (2012) 1896, arXiv:1111.6097.

[33] R. Brun, F. Rademakers, ROOT: an object oriented data analysis framework, Nucl. Instrum. Methods Phys. Res., Sect. A 389 (1997) 81.

[34] I. Antcheva, et al., ROOT: a C++ framework for petabyte data storage, statistical analysis and visualization, Comput. Phys. Commun. 180 (2009) 2499, arXiv:1508.07749.

[35] A.L. Read, Presentation of search results: the CL(s) technique, J. Phys. G 28 (2002) 2693.

[36] J. de Blas, M. Chala, M. Perez-Victoria, J. Santiago, Observable effects of general new scalar particles, J. High Energy Phys. 04 (2015) 078, arXiv:1412.8480.

[37] F. del Aguila, J. de Blas, M. Perez-Victoria, Electroweak limits on general new vector bosons, J. High Energy Phys. 09 (2010) 033, arXiv:1005.3998.

[38] LHCb collaboration, Measurement of form-factor-independent observables in the decay $B^0 \to K^{*0}\mu^+\mu^-$, Phys. Rev. Lett. 111 (2013) 191801, arXiv:1308.1707.

[39] LHCb collaboration, Test of lepton universality using $B^+ \to K^+\ell^+\ell^-$ decays, Phys. Rev. Lett. 113 (2014) 151601, arXiv:1406.6482.

[40] LHCb collaboration, Differential branching fractions and isospin asymmetries of $B \to K^{(*)}\mu^+\mu^-$ decays, J. High Energy Phys. 06 (2014) 133, arXiv:1403.8044.

[41] LHCb collaboration, Angular analysis and differential branching fraction of the decay $B_s^0 \to \phi\mu^+\mu^-$, J. High Energy Phys. 09 (2015) 179, arXiv:1506.08777.

[42] LHCb collaboration, Angular analysis of the $B^0 \to K^{*0}\mu^+\mu^-$ decay using 3 fb^{-1} of integrated luminosity, J. High Energy Phys. 02 (2016) 104, arXiv:1512.04442.

[43] Belle collaboration, Lepton-flavor-dependent angular analysis of $B \to K^*\ell^+\ell^-$, Phys. Rev. Lett. 118 (2017) 111801, arXiv:1612.05014.

[44] LHCb collaboration, Test of lepton universality with $B^0 \to K^{*0}\ell^+\ell^-$ decays, J. High Energy Phys. 08 (2017) 055, arXiv:1705.05802.

[45] ATLAS collaboration, Search for excited electrons singly produced in proton–proton collisions at $\sqrt{s} = 13$ TeV with the ATLAS experiment at the LHC, Eur. Phys. J. C 79 (2019) 803, arXiv:1906.03204.

[46] P. Kozów, The W and Z scattering as a probe of physics beyond the Standard Model: Effective Field Theory approach, Ph.D. thesis, Warsaw U., 2019, arXiv:1908.07596.